RESEARCH ARTICLE

Hawaiian fissure fountains 1: decoding deposits—episode 1 of the 1969–1974 Mauna Ulu eruption

C. E. Parcheta · B. F. Houghton · D. A. Swanson

Abstract Deposits from episode 1 of the 1969–1974 Mauna Ulu eruption of Kīlauea provide an exceptional opportunity to study processes of low intensity Hawaiian fissure fountains. Episode 1 lava flows passed through dense forest that had little impact on flow dynamics; in contrast, the pattern of spatter preservation was strongly influenced by the forest (through the formation of tree molds) and the preexisting topography. A low, near-continuous spatter rampart is present upwind and upslope, on the north side of the fissure. Most of the pyroclastic products, however, fell downwind to the south of the fissure, but little was preserved due to two processes: (1) incorporation of proximal spatter in rheomorphic lava flows 10–20 m from the vents, and (2) the downslope transport of cooler spatter falling on top of these flows beyond 20 m from vent. The lava flow field itself shows a complex history. Initially, discharge from the fissure exceeded the transport capacity of the southern drainage pathways, and lava ponded dynamically to a maximum height of 4 m for 40–120 min, until fountains began to decline. During declining discharge, lava flowed both southward away from the fissure and increasingly back into the vents. There is a clear "lava-shed" or delineation between where lava drained northwards back into the fissure, and where it continued flowing to the south. The 1969 deposits suggest that care is needed when products of less well-documented eruptions are analyzed, as postdepositional transport of spatter may preclude the formation of classic paired (symmetrical) ramparts.

Introduction

Hawaiian fountains are the low intensity end-member in the spectrum of sustained explosive volcanic eruptions. They produce basaltic lava flows and construct cones or linear steep-sided accumulations (ramparts) of typically agglutinated spatter. Cones form during eruptions with a dominant single source, circular vent, whereas ramparts form along sublinear fissure segments within fissure systems that are hundreds of meters to several kilometers in length. Asymmetry of spatter cones, associated with single vents, is common and well documented, driven either by downwind advection of the spatter (e.g., Puʻu ʻŌʻō in 1983–1986; Heliker et al. 2003) and/or by pre-existing topography (Kīlauea Iki 1959; Richter et al. 1970). Spatter rampart geometries are far less well described, but include both single ramparts and pairs of ramparts, symmetrically distributed along a fissure. Individual fountaining episodes at Kīlauea volcano have a range of durations from 2 h (Richter et al. 1970) to 16 days (Heliker et al. 2003) and eruption rates from 400 kg/s (Macdonald et al. 1983)–0.15 m^3/s to 1.7×10^6 kg/s (Richter et al. 1970)–641 m^3/s. The range of maximum-recorded fountain heights is 8 m (Heliker et al. 2003) to 579 m (Richter et al. 1970). Hawaiian fountains subdivide into high (>100 m) fountains with high mass discharge rates associated with point sources, and low (<100 m) fountains often linked to fissure sources and low mass eruption rates per unit length of fissure.

C. E. Parcheta (✉) · B. F. Houghton
Geology and Geophysics, University of Hawaiʻi at Mānoa,
Honolulu, HI, USA
e-mail: parcheta@hawaii.edu

D. A. Swanson
Hawaiian Volcano Observatory, U.S. Geological Survey,
Hawaii National Park, HI 96718, USA

Previous workers (e.g., Wilson 1980; Wilson and Head 1981; Vergniolle and Jaupart 1990; Parfitt and Wilson 1995; Parfitt et al. 1995; Vergniolle and Mangan 2000; Slezin 2003; Parfitt 2004) have modeled point-source fountains and estimated magma ascent rates of 0.2–14.6 m/s (Wilson and Head 1981). However, Hawaiian fountains are commonly fissure-fed for part or all of an eruption, as seen at Pu'u 'Ō'ō in 1983 (Wolfe et al. 1988); Izu-Oshima in 1986 (Sumner 1998; Aramaki et al. 1988); Etna in 1991, 1999, 2001, and 2008 (Stevens et al. 1997; La Delfa et al. 2001; Behncke and Neri 2003; Bonaccorso et al. 2011); and Eyjafjallajökull in 2010 (Moune et al. 2012). Aside from work done in the early 1980's (Wilson 1980; Wilson and Head 1981), models, to date, do not consider eruptions from a fissure or variability in fountain height and mass discharge rate along such a source. This study provides new information on the diversity of processes in Hawaiian fissure fountains by considering a well-exposed deposit from the 1969–1974 Mauna Ulu episode 1 (Fig. 1), which provides an opportunity to quantify the geometries of spatter ramparts and infer the interactions with coeval lava flows. A companion paper will address the vents and subsurface fissure system from the same eruption. Our aim is that data in this and the companion paper

can be used to expand future computational models of Hawaiian fountains to include fissure sources with variability of the eruptive system at several levels. This eruption episode provides an opportunity to study and quantify a low-intensity fissure eruption, with preservation of both the fissure and proximal eruption products. Rampart height, fountain spacing, and the distribution of lava flows versus agglutinated spatter around the fissure allow us to interpret how deposits vary with discharge rate and local environment.

The 5-year-long Mauna Ulu eruption of Kīlauea (Fig. 1a) was initiated by an episode of fissure fountains on May 24, 1969 (Swanson et al. 1979; Tilling et al. 1987). Nine hundred meters of the originally 4.5 km long fissure system remains accessible, unaffected by contemporaneous and subsequent Mauna Ulu lava flows. Eyewitness accounts (Swanson et al. 1979) indicate that the Mauna Ulu fissure system (Fig. 1b, red line), preceded by a propagating earthquake swarm, opened at 04:45 am Hawai'i Standard Time east of the old Chain of Craters Road. (We refer to the Mauna Ulu fissure system simply as "the fissure" even though it is not a single continuous feature). Rapidly opening, the fissure extended 2.5 km in 15 min (by 05:00), from 200 m north of Alae Crater in the east to the old Chain of
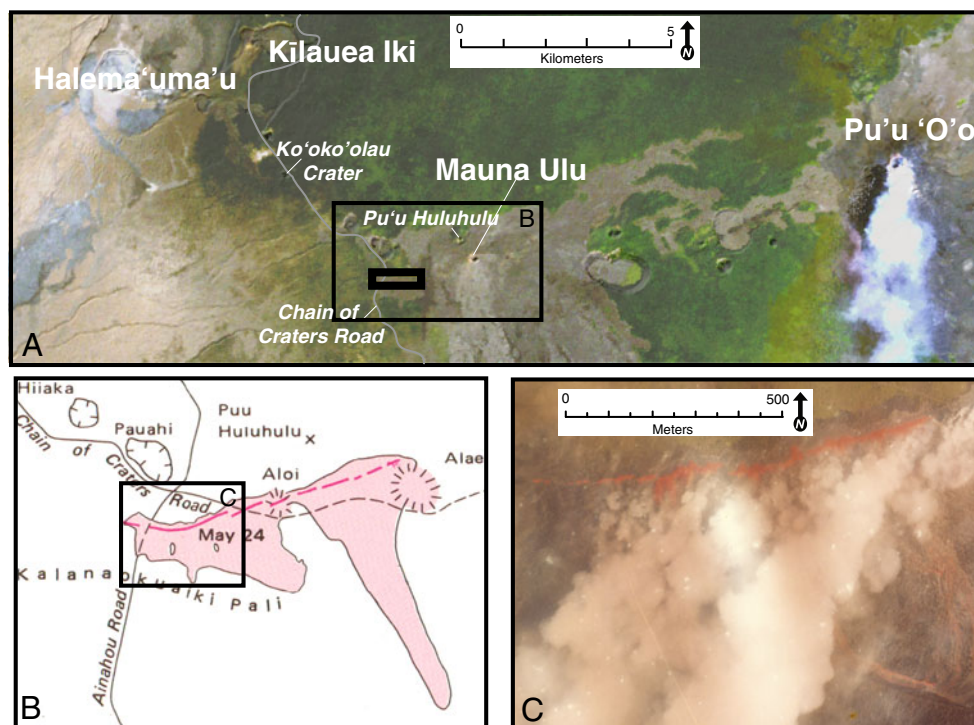

Fig. 1 a Satellite image of Kīlauea, Hawai'i. Major locations (Halema'uma'u, Kīlauea Iki, Mauna Ulu, Pu'u 'Ō'ō) are labeled. The present-day Chain of Craters Road is labeled, and denoted with *gray line*, and locations of high points mentioned in text (Ko'oko'olau Crater and Pu'u Huluhulu) are labeled. *Thin black box* labeled "*B*" designates area covered in **b**. *Thick black box* west of Mauna Ulu shield denotes the field area. **b** Modified map from Swanson et al. (1979). *Red line* is the episode

1 fissure and *pink-shaded area* is the extent of lava flow fields. This map indicates the old Chain of Craters road and Āinahou Road. *Box* labeled "*C*" is extent of area covered by photo in **c**. **c** Previously unpublished aerial photo from Sandia Labs at 09:40 Hawai'i Standard Time on May 24, 1969. Photo taken 1 h after fissure reaches full length. Note the flow field is fully developed (*lower right*)

Craters Road in the west, intersecting Ālo'i Crater (Fig. 1b). The fissure crossed the former 'Āinahou Road (current Chain of Craters Road) at 08:30. Initially, the whole fissure length hosted low fountains ≤50 m high, but rapidly evolved into two fountaining zones: an eastern zone (EZ) between 'Alae and 'Ālo'i craters, and a western zone (WZ, our field area, Fig. 1c) between Chain of Craters Road and 'Āinahou Road, separated by an inactive region 1 km long, through 'Ālo'i Crater. The low fountains showed small, but largely undocumented, temporal, and spatial variations in height.

Both fountaining zones fed lava flows that moved down a gentle southward slope, described in Swanson et al. (1979). During the 17.25 h of activity at the WZ, flows were impounded 1.2 km downslope by Kulanaokuaiki Pali, a north-facing fault scarp. Swanson et al. (1979) calculated that a total magma volume of 4×10^6 m^3 was erupted on May 24–25; no separate estimate was made for the EZ or WZ.

The eruption's ensuing 11 high-fountaining episodes and three effusive stages through 1974 is well documented (Swanson et al. 1979; Tilling et al. 1987), but little more is published about episode 1 (Peterson 1969; Swanson et al. 1971). This paper reconstructs the WZ events of May 24 from a physical volcanological perspective to (a) determine the intensity and variability in fountain behavior and coeval lava flows within a short-lived fissure system; (b) document the interaction between fountaining, lava flows, and drainback of dynamically ponded lava; and (c) determine how the forest, ground slope, and flow dynamics affected rampart growth and preservation.

Field area and methods

Field area

Discontinuous spatter ramparts from the WZ (Fig. 2a) strike 080° in a 900 m long, 30 m wide region across the northern part of the field area. Lava flows from the fissure extend horizontally 50 m upslope (north) and 200 m downslope (south) to a presently 1–2.5 m wide, 400 m long non-eruptive crack (labeled as "April 1970" in origin in plate 1; Swanson et al 1979), then another kilometer southward to Kulanaokuaiki Pali. Data were collected within a 250×900 m area bounded by the outer edge of the lava flows in the north and the non-eruptive crack in the south. A reference point of origin for the fissure was taken as the westernmost exposed vent and is the location from which distances in the paper are measured (Fig. 2a, yellow star). Based on rampart continuity and en echelon offsets between groups of vents, we divided the fissure into five segments (Fig. 2a, Table 1), labeled as I–V from west to east.

A 1965 contour map of the pre-eruptive Mauna Ulu region was digitized, and five small lava flows erupted in the area of interest between 1965 and May 1969 were added to produce a 0.5 m resolution pre-eruptive topography of the Mauna Ulu area (Fig. 2b). This pre-eruptive topography was then subtracted from the current digital elevation model to obtain the thickness of lava preserved in the WZ (Fig. 2c). Syn-eruptive (maximum lava height) and post-eruptive (current ground surface) topography was derived from a series of kinematic GPS transects (0.1 m resolution) both parallel and orthogonal to the fissure (Fig. 2d).

Characterizing rampart geometry and tephra dispersal

Rampart transects at 40 northern and two southern locations were made with a tape and compass. Each transect orientation was perpendicular to the steep inner rampart wall, and length measurements and slope angles were measured with the aid of a straight line guide. A cross-sectional rampart area was calculated by drawing the profile for the transect and dividing it into a series of polygons based on obvious changes in rampart slope (Fig. 3c) that could then be converted into 1-m-wide unit volumes. Pre-eruption ground slope was measured from the digitized pre-eruptive DEM, approximated as a single triangle at the base of the rampart cross sections, and subtracted from the volume calculated for each 1-m-wide transect. Spatter dispersal was estimated from slope measurements of the outer rampart and quantified through calculations of deposit thinning half distances (Pyle 1989). In addition, thinning half-distances were calculated for two transects through aligned spatter mounds south of the fissure where relics of widespread tephra fall were preserved.

Characterizing lava flow directions, volumes, and stagnation times

Lava formed a pāhoehoe flow field in which the following features were analyzed: large-scale drainage pathways, local flow directions, prominent flow features (i.e., bow waves and wakes), lava crust thickness, heights/locations/thicknesses of lava shelves, maximum lava inundation heights, and localized ground slopes derived from pre- and post-eruptive elevation changes. Lava cooling times (t) were calculated from average crustal thickness measurements (c) for a range of features (Hon et al. 1994):

$$t = 164.8\left(c^2\right) \qquad (1)$$

The reconstructed flow thickness data (Fig. 2b) were used to calculate the lava volume that remains on the surface, i.e., total erupted lava volume less the amount of lava that drained back into the fissure.
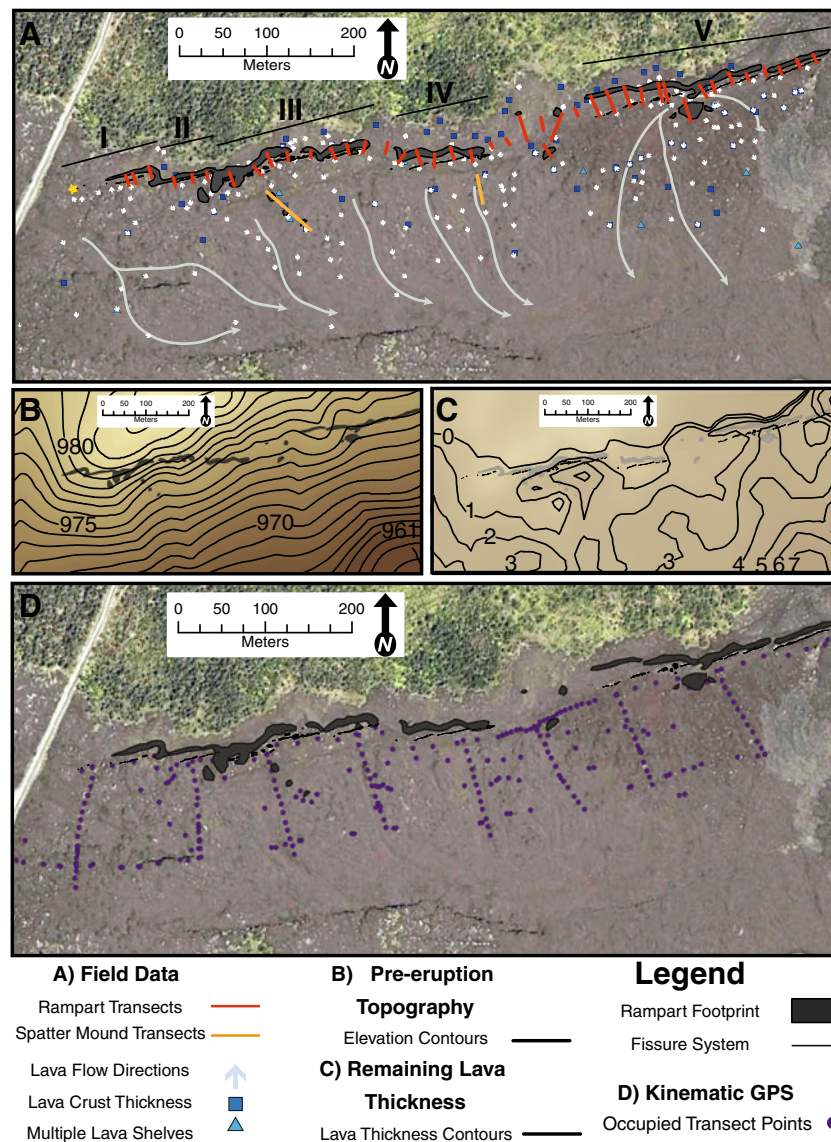
Fig. 2 Location maps of datasets. In **a** and **d**, *green* forest north of the fissure, *dark gray* lava flow field, and the road cutting the upper left corner is the old Āinahou Road/new Chain of Craters Road. The *dark, linear feature* at the *bottom* of the photograph is not Kalanaukuaiki Pali, but instead an open crack along a low, north-facing fault scarp. Segments of the fissure are labeled I–V. Rampart footprint (dark gray) and the fissure (black, immediately south of ramparts) are superimposed. **a** *Red lines* across the ramparts are locations of rampart transects 1–40 on the northern side, numbered from west to east, transect 41 on the western southern rampart, between segments IV and V, and transect 42 on the eastern southern spatter rampart, in the middle of segment V. *Dark blue squares* are locations of crustal thickness measurements, *cyan triangles* indicate multiple lava shelves, *small white arrows* are flow direction measurements (pointing in the direction of flow), and *long gray arrows* indicate lava drainage pathways. *Yellow star* is the western most vent, and will be the reference point of origin from which distances to other features in the text are measured from. **b** Digitally created pre-eruption surface topography with the rampart footprint superimposed. **c** Contours of present-day lava thickness remaining on surface (i.e., lava erupted from WZ, not including drainback) up to 120 m south of the fissure. **d** Locations of occupied positions for kinematic GPS transects

Eruption observations

Visual documentation of the May 24, 1969 eruptive activity is limited to four aerial photos from Sandia Labratories and 19, previously unpublished, 35-mm slides taken by Hawaiian Volcano Observatory (HVO) staff member Jeffrey B Judd (JBJ). No film footage was taken on that day. Moreover, aside from the mean fountain height estimate, total eruption volume, and eruption rate calculations, no other recorded measurements were found pertaining to May 24 and episode 1. Data presented in this section are derived from a subset of the available photographs, while all published information and unpublished photographs were utilized in the reconstruction of events, which is discussed in the interpretations section.

An eruptive fissure panorama could be created from three JBJ photographs, designated in their captions as "PM"

Table 1 Table showing the length, orientation, and distance from the reference point (yellow star (Fig. 2a)) for each fissure segment in the field area and the gaps between them. The number of vents along each fissure segment is also listed

Name	Orientation (°)	Vents	Length (m)	Start distance from origin (m)	End distance from origin (m)
I	80	1–8	82	0	82
II	80	9–13	39	107	150
III	75	14–33	161	168	336
IV	82	34–40	111	361	475
V	79	41–54	257	600	875
Gap A-B	95	N/A	32	82	107
Gap B-C	132	N/A	25	150	168
Gap C-D	108	N/A	32	336	361
Gap D-E	78	N/A	129	475	600

(afternoon), taken from an unspecified northern location. Based on spatial orientation of eruption plumes, and Pu'u Huluhulu's silhouette, we determined that the panorama was taken from Ko'oko'olau Crater's spatter cone and that the eastern fountains are blocked from view. Western fountain heights visible above the forest were determined by a simple geometric ratio of height (h) over distance (D) :

$$\frac{h_{Pu'uHuluhulu}}{D_{Pu'uHuluhulu}} = \frac{h_{fountain}}{D_{fountain}} \qquad (2)$$

Forest vegetation consisted predominantly of 10 m tall mature Ohi'a lēhua (*Metrosideros polymorpha*) trees, which we added to the measured height of each fountain from the photograph for a better estimate of total fountain height.

Corrected fountain heights ranged between 13 and 32 m. Our measurements correlate well with Swanson et al. (1979), who stated that the WZ had maximum eruption heights of 50 m. Variations of 10–15 m in fountain height are seen over lateral distances as short as 4–15 m. High, optically dense fountains in the photograph are either single sources or, at most, clusters of three to four vents over a few tens of meters. The visible fountains were triangulated to be from fissure segments III, IV, and V relative to the locations of Pu'u Huluhulu, 'Āinahou Road, and the location of the photographer.

Weak low fountains or strong continuous spattering are seen above ramparts in the remaining 16 JBJ photographs on May 24. Lack of scale, problems of perspective, and not seeing the base of the fountain preclude measurements of absolute fountain heights from these images. Photos from early afternoon provide a wide view of activity, with one image capturing eight spattering sources varying in fountain height and optical density. Relative height fluctuations were determined by comparing the size of the photo's largest airborne clasts to the equivalent mean maximum clast dimensions measured on the ramparts (37×19×7 cm). Fountains were calculated to vary between 0.2 and 5 m above the rampart crests even though absolute height is uncertain, but are likely not to exceed 8–12 m given the final rampart heights (heights discussed in next section).

Rampart geometry and tephra dispersal

Rampart deposits, tephra dispersal, and pyroclast vesicularity

Agglutinated spatter ramparts are nearly continuous on the northern side of the fissure but are present along only two
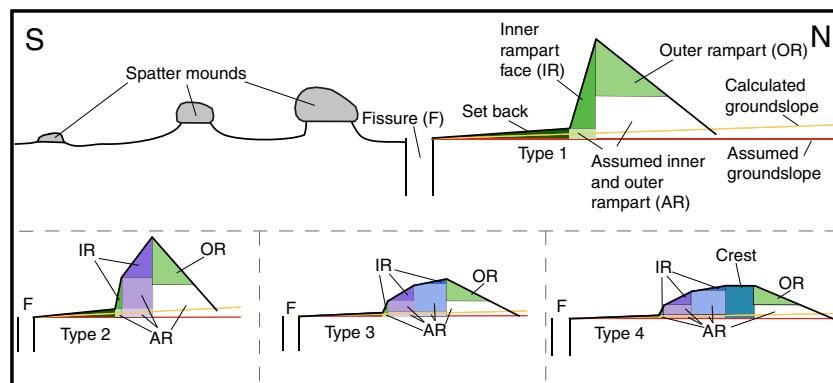

Fig. 3 Cartoon cross-section of agglutinated spatter deposits. North is to the right of the figure. Cross-sections measured the set back distance (fissure to base of the inner rampart) and inner and outer rampart faces (*darker triangles*). Volume calculations account for presumed spatter (*lighter squares*) that could not physically be touched, and initially used a flat ground slope (*red line*), but were corrected (*yellow line*) after Fig. 2d was generated. *Top*: Full representative cross-section. To the south, spatter mounds are present; to the north, a type 1 rampart (most common) that has 1 inner rampart face. *Bottom*: half cross-sections of rampart variations: *left*: type 2 rampart (two inner rampart faces), *middle*: type 3 rampart (three inner rampart faces), and *right*: type 4 rampart (three inner rampart faces and a flat crest)

segments on the southern side, along with infrequent small spatter mounds (Fig. 2). We have documented four types of rampart profiles (Fig. 3). Table 2 and Fig. 4 summarize mean and range of parameter values for each type, respectively. Rampart geometry 1 (having one inner rampart face and one outer rampart face, with no flat crest) makes up 86 % of the rampart transect geometries in the field area.

The linear half-distance of pyroclastic fall deposits (distance over which the outer wall of the deposit halves in thickness) scales with mass eruption rate (Pyle 1989; Wilson and Houghton 2000). Half-distance values of the northern ramparts are less than 10 m (Fig. 5). No distal tephra blanket is present to the north. A single measurement of thinning half distance of the southern proximal ramparts is 11 m. Two transects of southern aligned spatter mounds perpendicular to the fissure yield distal thinning half distances of 21 and 15 m. These data constrain clast dispersal beyond the ramparts, representing what is preserved of a widespread "tephra blanket" segment of the deposit. All the data are compatible with Hawaiian/Strombolian dispersal in the sense of Walker (1973) and Pyle (1989).

Intense welding and rheomorphic flow precluded us from constraining clast geometries along most of the ramparts. One exception is at a site at 155 m, on the west side of segment III, where clasts show no evidence of rheomorphism. Here, maximum pyroclast dimensions were measured in situ, as broadly representative of the rampart grain size (Fig. 6a), averaging $15 \times 10 \times 10$ cm (range, 2–54 cm wide and 1–15 cm thick). Along the rest of the fissure, pyroclasts margins are rheomorphic (Fig. 6b) and strongly agglutinated within tens of centimeters of the rampart exterior. In extreme cases, e.g., at the 466 and 650 m locations, pyroclasts are completely welded and indistinguishable throughout the interior portions of the broken ramparts. Agglutinated spatter on the rampart exterior contains very sparse but larger vesicles, typically 6×4 cm. A true diameter of the largest vesicles (>12 cm) could not be obtained because the clasts are broken and incomplete. Vesicle textures of pyroclasts in the interior of broken northern ramparts (distances, 466, 650, and 707 m) include a mixture of stretched and spherical vesicles. Spherical vesicles are typically 0.30–0.35 cm in diameter (largest vesicle, 2 cm long and 1 cm wide), and sheared vesicles are typically 0.6×0.2 cm (largest

1.4 cm long and 0.6 cm wide, Fig. 6c). A separate population of smaller, dense, vesicle-poor fluidal nonwelded spatter particles surround many vents and are dispersed for only a few meters about the vent.

Northern ramparts

Agglutinated spatter ramparts are present upwind and upslope of the fissure for 80 % of the fissure length between distances of 36–347 m (segments I, II, and III), 368–470 m (segment IV), 554–564 m (between segments IV and V), and 598–887 m (segment V). Parameters that vary along the fissure length include the height, outer rampart slope, rampart setback from the fissure, and the abundance of tree molds. Rampart height, i.e, maximum deposit thickness, varies along the fissure, ranging from 70 cm to 7.1 m with a mean of 4.4 m. Height variation on the order of 1–2 m occurs over length scales of 2–3 m along the length of the fissure. Outer rampart slope, which reflects the thinning rate and thus mass discharge rate (Walker 1973; Pyle 1989), ranges from 0 to 37° with a mean of 21°. Segment II ramparts (transects four to six) are the only ones close to the fissure (ca. 1 m), otherwise the base of a rampart is set back significantly from the fissure, typically 10 m but ranging between 3 and 30 m. Tree molds are present within a broken rampart at a distance of 560 m, but obvious signs of tree branches or trunks are not present on the remaining ramparts' surfaces (or the outer surface of the broken rampart). Tree molds are also present immediately east and west of the broken rampart between distances of 575–657 m, where northern ramparts are non-existent. In addition, tree molds can be found between distances of 342–370 m (segments III and IV), as well as within a 40 m radius of the westernmost vent.

Southern ramparts and spatter mounds

Agglutinated spatter ramparts are found in only two locations on the southern side of the fissure (constituting 5 % of exposed fissure length): between distances of 529–548 and 694–721 m. These two rampart segments are each perched at dividing points between major lava pathways (see "Lava

Table 2 Rampart types separated into their frequency and mean geometric constraints

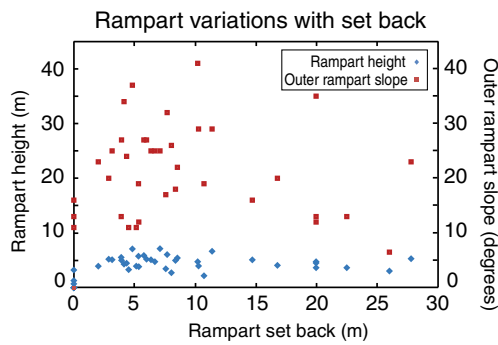| Rampart geometry	Frequency (%)	Mean rampart transect volume (m³)	Mean rampart height (m)	Mean rampart width (m)	Mean outer rampart wall length (m)	Mean outer rampart wall slope (°)
Type 1	86	0.37	4.5	15.58	5.81	21
Type 2	7	0.31	4.0	13.36	4.19	35
Type 3	2	0.32	4.7	12.37	4.52	25
Type 4	5	0.59	4.3	23.74	3.57	15

Fig. 4 Plot showing relationship of rampart height (*blue diamonds*) and outer slope (*red squares*) to the set back distance. Data points on the *y*-axis (*x*=0) have no vent exposed at the rampart location. Data points on the *x*-axis (*y*=0) have no rampart associated with vent exposure

flows" section). There are numerous isolated small spatter mounds associated with tree molds on the south side of the fissure to distances of 100 m, i.e., well beyond where the ramparts should have formed.

Lava flows

The first lava flows from the WZ fissure engulfed 5 km^2 of land immediately surrounding and downslope of the fissure
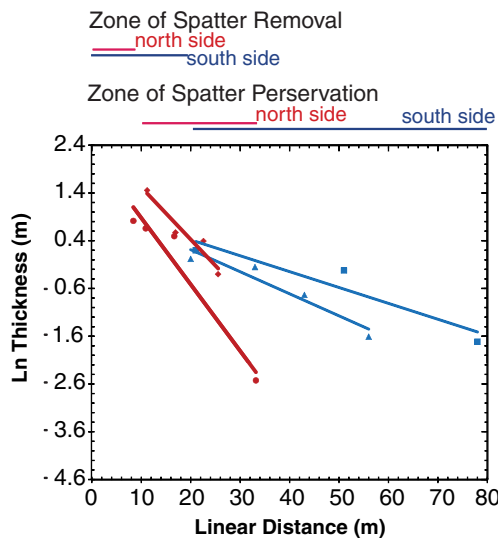

Fig. 5 Plot of thickness vs. distance perpendicular to the fissure of two full transects. Northern rampart transects (*red*) show a thinning half-distance of 6 m in the west (*shallower line*) and 5 m in the east (*steeper line*), with projected heights of 14 and 10 m at the vent, respectively. Southern spatter transects (*blue*) show a thinning half distance of 21 m in the west (*shallower line*) and 15 m in the east (*steeper line*) with a maximum projected deposit thickness of 3 m at the vent in both cases. Breadths of spatter preservation and removal zones are shown above the plot. The zone of spatter preservation is the range over which spatter was deposited, but was not always and could have been preserved. The R^2 values for all lines range from 0.89 to 0.95

(Swanson et al. 1971). While a velocity was not estimated for the flow front, the lava field had clearly reached Kulanaokuaiki Pali, 1 km south of the fissure, in the aerial photographs (Fig. 1c) at 09:40. We assume that fountains fed lava flows continuously between the onset and 09:40, thus allowing calculation of minimum flow front velocities: 0.15 km/h at the old Chain of Craters Road and 0.4 km/h at the old Āinahou Ranch Road. During episode 1, EZ and WZ produced a combined 4.5×10^6 m^3 of erupted lava at an average rate of 40 m^3/s (Swanson et al. 1979).

Paleoenvironment: pre-eruption forest and tree molds

A dense forest originally stood where the lava fields are now located (Swanson et al. 1979), and many, but not all, of these trees became lava tree molds. We have digitized the pre-eruptive ground slope (Fig. 7a) and 5,003 pre-eruption trees from aerial photographs, 557 of which have been mapped as tree molds in satellite imagery or using handheld GPS (Fig. 7b). It is clear from pre-eruptive aerial photographs that, while tree density did vary slightly, there was no clear "path of least resistance" for the lava to flow through. Figure 7b shows over 400 mapped tree molds on the south side of the fissure, which typically have a vertical lava veneer 0.1–0.25 m thick and a total mold diameter of 0.5–0.75 m. The widest tree mold (at 803 m distance and 20 m south of the vent) is 2 m across at the base, but is unbroken, so the lava veneer thickness and internal diameter are unknown. Tree molds located directly adjacent to vents are short and rounded, less than 0.5 m in both height and diameter. The tallest tree mold (Fig. 7c) at 155 m distance is 1.5 m high, with a 1-m wide base. The mold itself consists of spatter around a single tree encased in 13 cm of lava (thickest observed in the field area). In several places, small trees that were closely spaced together initially formed individual tree molds, but as the lava continued flowing they merged into a composite mold and forced later lava to flow around the composite structure (Fig. 7d). Large composite tree molds have prominent elevated "bow waves" and elongated wakes. Molds of several tree branches are contained within one broken rampart, but it is unknown whether the remaining ramparts also contain molds of tree branches. Spatter topped tree molds occur within 100 m south of the fissure. On these tree molds, and other topographic high points, there are often several levels of lava crusts projecting outward as shelves. Three (±1) lava shelves are common on tree molds and paleo-highs near the fissure system and pairs of shelves are present on tree molds and the drainage pathway margins farther from the fissure system. Depth to the pre-eruptive ground surface was measured in 10 of the southern tree molds with a mean maximum inundation height (top of tree mold to pre-eruptive ground surface) of 1.8 m. Tree molds

Fig. 6 a Photo of weak agglutinated pyroclasts that retained individual identities with no rheomorphism (at 155 m distance). Some clasts are outlined to show complexity of rampart growth. We measured the x- and z-dimensions (assuming $x=y$ in the depositional plane). The measured z-dimension is perpendicular to the depositional surface. **b** Photo of spatter on inner rampart face at 707 m distance. Clast identities were retained, with 4 hatched in red for emphasis. Rheomorphism was in direction of arrow, down the rampart face towards the vent. **c** Clast (outlined in *red*) just under surface of inner rampart face at 707 m distance. Vesicles (*yellow*) are both sheared and nonsheared. Sheared vesicles are elongate both normal to the direction of impact flattening and parallel to flow direction, and are present in the middle of clast above pen. More spherical bubbles are on the *left* and *right* sides of clast
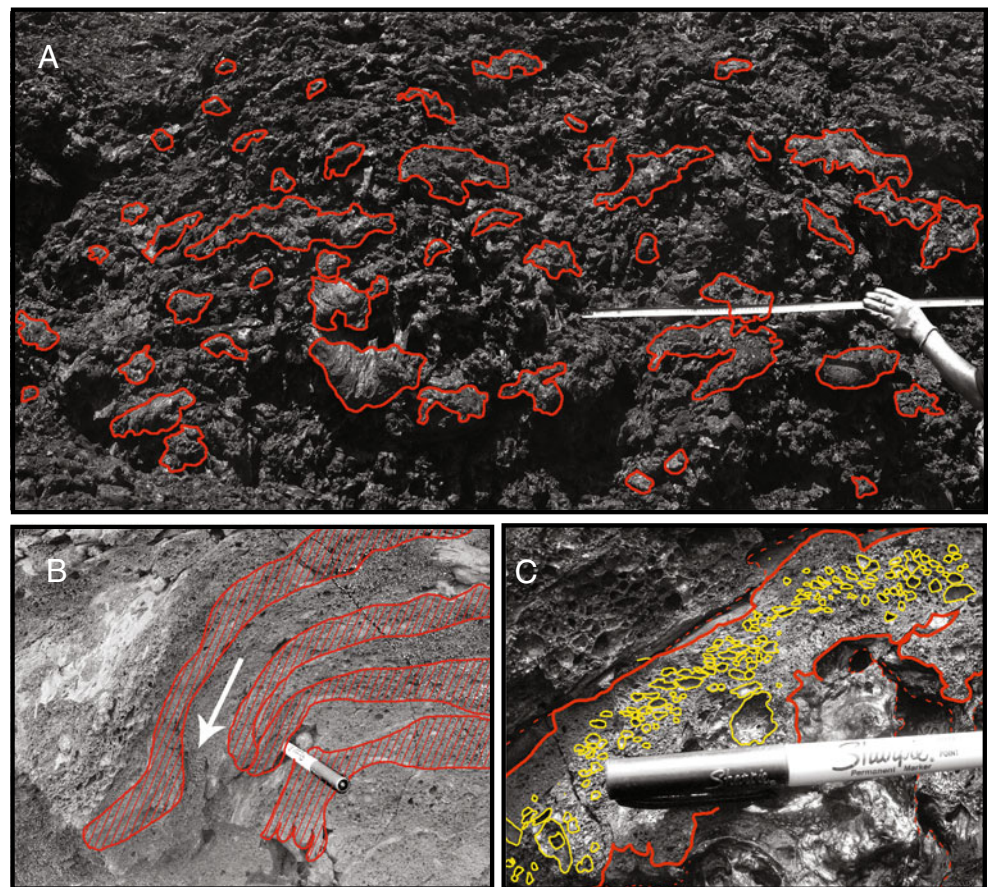
closest to the fissure have shallower depths (~1 m) than those farther downslope (~2+m).

Flow directions and pathways

Most lava drained south from the fissure, following the regional slope. There are six preserved topographic lows (Fig. 8a) south of the fissure, corresponding to major lava pathways within the flow field, each oriented to the south (Fig. 2). Close to the fissure, pathways have lateral, margin parallel, ropy folds where thin, newly formed crust was stranded on the flow margins. Southern lava pathways bend eastward 120 m downslope of the fissure. Flow lineations in pathways (south and east) are consistent across the flow surface; a total of 181 flow direction indicators were recorded (Fig. 2, Table 3). Within southern lava pathways, flow indicators point consistently southward, but between the pathways, flow directions are highly variable. Immediately adjacent to and on both sides of the fissure, lava flow directions are inward toward the vents, where drainback textures are present.

In three locations on the north side of the fissure, volumetrically minor but dynamically important lava flows are present where ramparts are absent: the middle of segment III, between segments III and IV, and between segments IV and V.
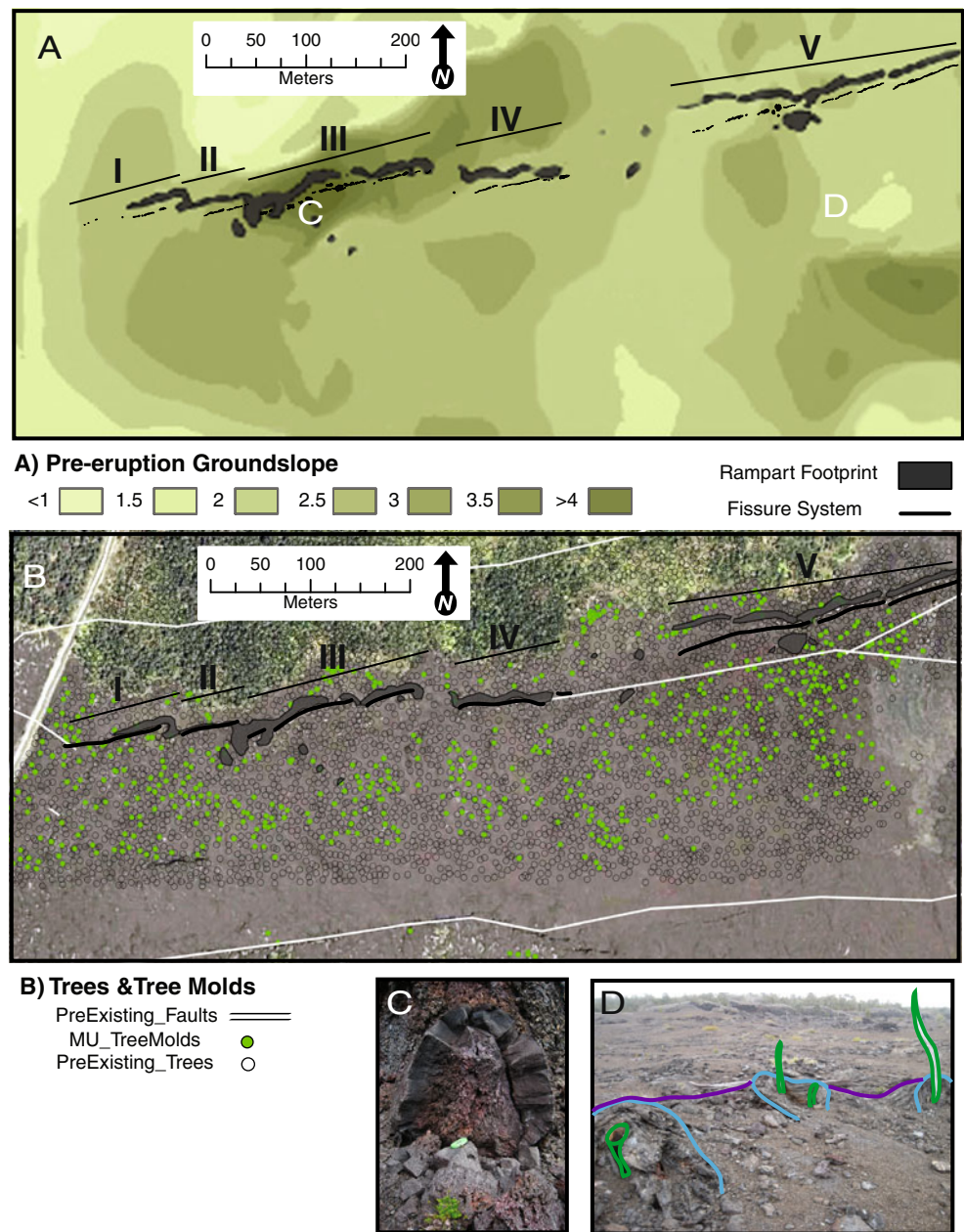
Observations from lava crusts

Lava crusts grow while in contact with underlying moving lava (Stovall et al. 2008) and their thicknesses, whether in the main pathway surfaces or as elevated lava shelves, allow us to determine cooling times following Hon et al. (1994; Table 3), which help define the durations of different stages in the evolution of the flow field.

Crustal thicknesses on the short flows north of the fissure average 10 (±4) cm, equivalent to 90 min of crustal growth (Hon et al. 1994). Areas between the major southern pathways show a wider range of crustal thickness up to 24 cm, equivalent to a maximum of 9.5 h (Hon et al. 1994). Drainage pathways crusts average 9 (±2) cm thick, equivalent to only 80 min of crust growth (Hon et al. 1994). Thin, inward-dipping, near-vent crusts that characterize drain back into the fissure at the end of the eruption are typically 5 (±1) cm thick, equivalent to 30 min of growth (Hon et al. 1994), although relative timings of drainback crusts across different vents are ambiguous.

Thicknesses of preserved lava shelves on topographic high points (Fig. 8b) record the durations of relatively stable conditions with matching discharge and drainage rates. Figure 2 shows the locations of all the shelf thickness measurements. The uppermost shelves preserved near the fissure are up to

Fig. 7 a Interpolated ground slope from topography in Fig. (2b) with ramparts and vents superimposed. *Darker shades of green* indicate steeper slopes, in gradations of 0.5°. *C* and *D* indicate locations of **c** and **d**. **b** Map of forest density and tree molds. *Circles outlined in black* are trees on pre-eruption aerial photos, *green circles* are tree molds mapped via field GPS and present-day satellite imagery. *White lines* are pre-existing faults, mapped from 1965 aerial images. More tree molds are preserved immediately south of the drainage divide than in the area of lava the reentered the fissure. **c** The tallest tree mold (1.5 m) in the area (segment III), unique in being initially constructed of spatter, then covered in lava veneer. **d** Image showing the growth of individual tree molds (*blue*) into a composite tree mold (*purple*), creating lava pathways by diverting lava around the trees (*green*). The three trees span 10 m

A) Pre-eruption Groundslope

<1 | 1.5 | 2 | 2.5 | 3 | 3.5 | >4

Rampart Footprint

Fissure System

B) Trees & Tree Molds

PreExisting_Faults
MU_TreeMolds
PreExisting_Trees

2.5 m above the pathway surface, and have 6–9 cm thicknesses correlating to 40–120 min of crustal growth (Hon et al. 1994). The lower crusts are generally thinner, from 4 to 10 cm, corresponding to 15–100 min of growth (Hon et al. 1994). Farther from the fissure, upper crust thickness and cooling times (7–9 cm, 48–80 min) are similar to proximal sites, but heights range up to 1.5 m above the pathway surface. The single lower shelf ranging 6–11 cm thick corresponds to 40–120 min of crustal growth (Hon et al. 1994). Elevation of the highest lava shelves gradually decreases southeastward across the field area from 996 m above sea level (asl) at segments I and II to 991 m asl south of segment V (Fig. 8c). In contrast, the final surface of the lava (current ground surface)

shows a complex pattern of late-stage draining. The boundary between the two different flow regions is plotted as a thin solid black line on Fig. 8d. The kinematic GPS height measurements (Fig. 2d) show the elevation of the highest lava shelves (Fig. 8c) and ground surface after draining (Fig. 8d).

Interpretation

Episode 1 in the WZ consisted of three phases: (1) a short interval of fissure propagation, waxing discharge, and lava inundation; (2) vigorous sustained fountains reaching maximum heights of 50 m with sustained and stable

Fig. 8 **a** Looking northwest, upslope one of the major drainage pathways. *White arrow* indicates direction of flow (south), and is placed in center of pathway. **b** Lava shelves with a meter stick for scale, crossing the lower shelf. Flow lineations are shown on the upturned crust between the meter stick and the backpack. **c** Satellite image of field area where forest and lava flow field are same coloration as Fig. 2a. Map contouring the elevation of the highest lava shelves, measured at the kinematic GPS locations shown. Elevation decreases to the south east in 1 m intervals. **d** Kinematic GPS-derived ground topography from transects shown in Fig. 2d. *Black squiggly line* is a "lava drainage divide" showing where present elevations indicate lava drained back into the fissure after fountain activity stopped (north) or continued into the flow field (south). The lowest elevation along the fissure is between segments IV and V
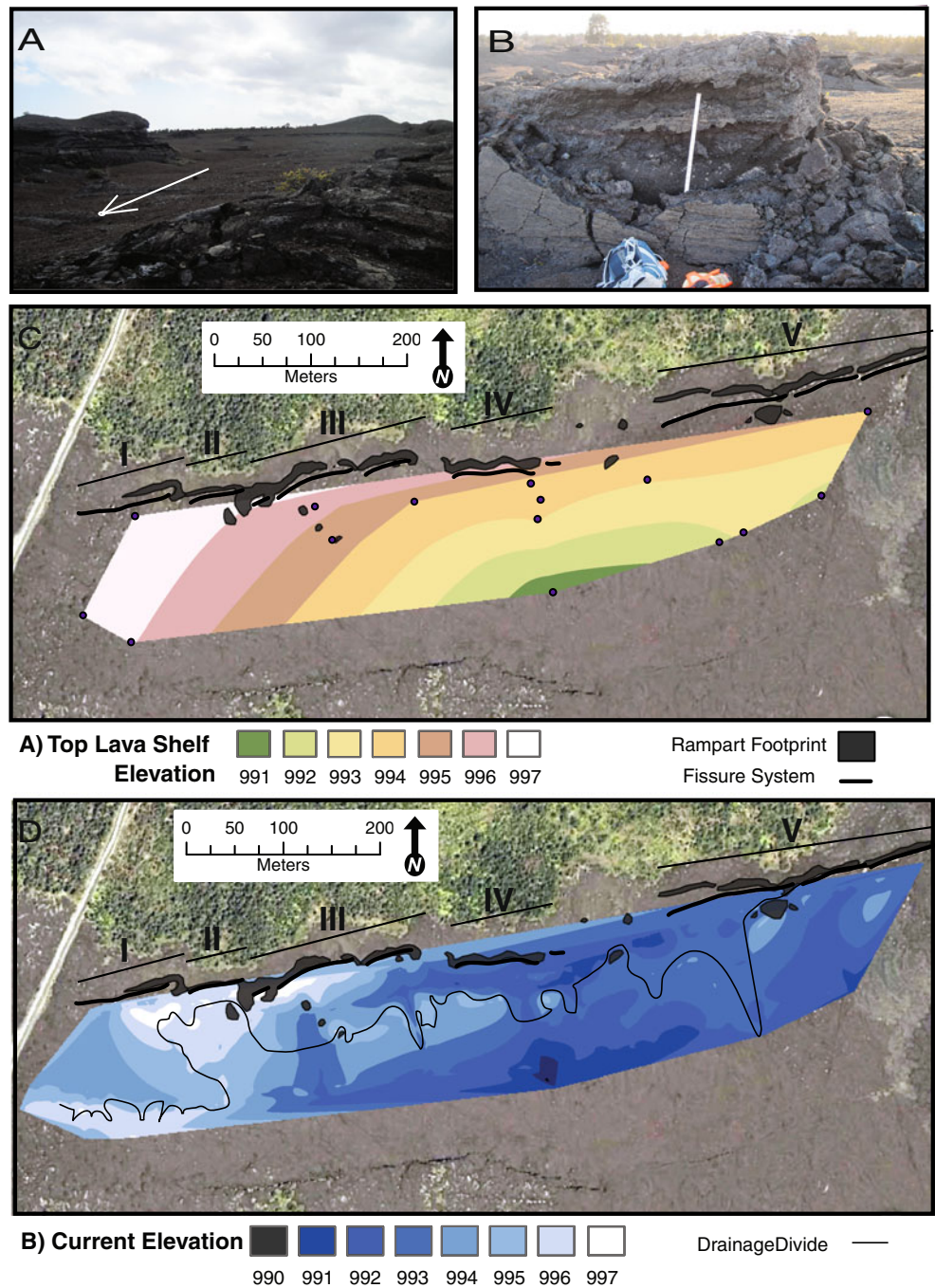
discharge and dynamic ponding of lava; and (3) waning discharge, discontinuous fountaining activity, and lava drainback into the fissure. There are no direct records, however, of the durations of these phases. Next, we discuss indirect ways of constraining these phases, as summarized in Table 4.

Table 3 Mean values of lava data, including flow directions, crustal thicknesses, calculated crustal growth/lava stagnation times, and shelf heights above the ground surface (where present)

Mean flow direction N of ramparts (°)	Mean Flow direction S of ramparts (°)	Mean lava crust thickness (cm)	Mean lava stagnation time (h)	Mean first lava shelf height (where present; m)	Mean second lava shelf height (where present; m)	Mean third lava shelf height (where present; m)
352	164	10	1.9	1.70	1.19	.72

Table 4 Revised and enhanced chronology of May 24, 1969

This table summarizes the physical processes that acted at various times during the 17.25 h of activity

Phase	Description	Duration (h)	Timing
1	Rapid growth of fissure, waxing discharge	3.5	04:45–08:30
2	Steady discharge, dynamically ponded lava	2–4	Onset 08:30–09:40
			End 12:00–13:00
3	Waning fountain activity, drainback	9	13:00–22:00

Eruption dynamics

The opening phase of the WZ eruptive activity was likely characterized by voluminous production of lava flows along the whole fissure due to the fact that the flow field was at full length and width by 09:40. The area between segments IV and V has the lowest pre- and post-eruption elevations, thickest lava crusts, and highest lava shelves (4 m) along the whole fissure, and has neither northern ramparts nor exposed vents. We suspect that these observations can be accounted for by a sustained effusion during phase 1 that flooded this low lying area, precluding nearby rampart formation during all phases. Along the entire fissure, tree molds formed as lava inundated the forest and continued to grow as long as the tree mold was submerged in lava. Rampart formation also likely began at this time, with spatter establishing a solid base north of the fissure and to the south on both paleo-topographic highs and around trees close to the fissure.

Our investigation into the lava features along the crack labeled in Swanson et al. (1979, plate 1) as "April 1970" indicates that the crack was open on May 24, 1969, and then reactivated in April 1970. The pre-eruption width of the crack is unknown due to vegetation in the aerial photographs, but flow textures suggest that lava initially flowed into it, but then bridged it and continued flowing down slope in phase 1, eventually ponding against Kulanaokuaiki Pali.

During peak flow (phase 2), all pre-existing paleotopographic highs within 20 m of the fissure were covered by at least 1 m of lava, but on average the lava surface was approximately 2.5 m higher than the present pathway surface. Figure 8c indicates that, at this time, the flow of lava was consistently downslope away from the fissure, and most of the flow was directed southeastward following preexisting ground surface. The lava was thus behaving as a dynamically ponded sheet flow with meter-scale variations in flow depth. Fountain height and intensity varied greatly, not only laterally along the fissure, but temporally. At this stage, fountains must have erupted through, and entrained, portions of ponded lava in the vents. High pyroclastic accumulation rates did not lead to rampart construction, especially in the south, as falling spatter in areas of lava drainage were carried away, apart from those pyroclasts which landed on tree molds. A small volume of lava flowed around the northern ramparts, covering the bases of the outer ramparts,

and has crustal thicknesses reflecting an early onset of crustal growth in a stable environment, suggesting growth contemporaneous with rampart construction. Lava trapped between the fountains and the inner walls of the northern ramparts undercut the rampart bases. We suspect this undercutting was thermal instead of mechanical, as the newly formed ramparts were likely a similar temperature to that of the lava ponded up against it, thereby decreasing the thermodynamic barrier needed to allow thermal erosion. We postulate that any broken and cracked ramparts may have been destabilized by this undercutting and subsequent removal of the lava support during the last eruptive phase. Tree molds record the maximum inundation height but give no direct growth duration as the cooling relation of Hon et al. (1994) cannot be used for the condition of lava crusts excluded from contact with the atmosphere.

Ultimately, after peak flux, the drainage rate away from the fissure exceeded the declining lava supply from the fountains (phase 3). The panorama photograph from Koʻokoʻolau Crater shows that activity waned inward from both ends of the WZ. The western-most fissure segment had the simplest and shortest history of inundation and drainage, and does not show a complex pattern of drainage during phase 3. Most lava continued to drain southward, but some began flowing back into those fissure segments that had ceased fountaining. Near-fissure crusts showing a lack of flow indicators reflect relatively passive drainback beneath fixed crusts at this time. Lava reentered the fissure along its entire length after fountain activity stopped locally. At this time, southward flow focused within the major pathways and surface flow indicators formed. Lava shelves gauge periods of relatively constant lava flux as opposed to periods of actively waxing or waning flow. The presence of multiple lava shelves suggests that the waning discharge rate was incremental with one or more periods of relative stability during the decline. A complex boundary exists between late-stage lava that drained back into the fissure and lava that continued to flow downslope (Fig. 8d).

Variability of fountaining along the western fissure

There must have been significant variation with time in the relative intensity of different vents, as high points on the ramparts are not always coincident with the highest fountains as seen in single photographs. In the extreme case,

images from old 'Āinahou Road looking to the east show high ramparts with no fountains, indicating an early high rate of accumulation and rapid rampart construction over a short period. Fountain intensity and height for those areas shown in the photographs were likely at a maximum early in the eruption, as they have comparable heights to other high ramparts, where photographs indicate peak activity occurred at a later time. However, the whole WZ did not erupt with equal intensity during the full 17.25 h of activity and rampart-derived, time-averaged eruption rates are therefore a minimum estimate of instantaneous eruption rates during fountain activity.

Chronology

Phase 1 (inundation and increasing fountain activity) lasted from 04:45 to 08:30, by which time the whole western fissure was active. Based on the literature and eyewitness reports, we assume that the WZ fountains began sequentially and rapidly, with the easternmost fountains starting up to 3 h before those in the west. We infer that phase 2 (peak flux) was underway by 09:40 since the aerial photograph indicates vigorous fountaining of all segments and a well-developed flow field. The highest lava shelves created during maximum inundation formed over a period of 40–120 min, a minimum estimate for the duration of phase 2. The duration of phase 3 (waning) can be estimated from the thickest crusts present between lava pathways to be approximately 9 h. This suggests the waning phase began around 13:00. We conclude that phase 2 had a duration of no longer than 4 h (~9:00 to ~13:00), ending between noon (in the west) and early afternoon (in the east).

In the far west, fountaining either did not take place from the fissure or had such low height, weak intensity, and/or short duration that any spatter deposits were subsequently buried by lava flows emanating from segments I and II. Segments I and II ceased fountaining next (certainly by early afternoon, before ground photographs were taken). Lava from segments III, IV, and V did not reach segments I or II. The gap between segments IV and V was likely to have been a major draining path for lava within the drainage divide, and probably died early (between late morning and mid afternoon), although this section has the most ambiguous timing estimates along the whole WZ. Fountain cessation here may have been induced by drowning (Wilson 1980), since this area was (and still is) the lowest topographic point along the fissure and would have contained the greatest depth of ponded lava in and above the vent. Given that fountains along segment V were weak or absent in the mid to late afternoon, we conclude that activity ceased here earlier than for segments III and IV. Drainage into segments III, IV, and V is unlikely to have started before late afternoon or early evening (i.e., until after the ground photos were

taken). We conclude that the gap between segments IV and V continued draining lava away from the fissure after all fountains had ceased because flow indicators point west toward segment IV where strong drainback textures cover the surface lava. Absolute elevation of this gap is lower than that of the vents in segment IV and the ground slope itself is dipping towards the gap between these two segments. Lava drainage in each fissure segment presumably ended in the order of segments I and II, by segment V, then segments III and IV, and finally ending in the gap between fissure segments IV and V.

An important conclusion drawn from the observations is that transitions between phases were not isochronous along the fissure. Lava almost certainly drained into some portions of the fissure while fountains still erupted from other portions of the fissure. At the end of all fountaining activity, lava reentered the fissure along its entire length.

Discussion: asymmetry and absence of ramparts during fissure eruptions

The May 24, 1969 spatter deposits reveal an interesting paradox. Spatter is preserved only locally south of the fissure, but our estimates based on the sparse preserved deposits, suggest that twice as much material fell in this downwind region than in the northern upwind region, which is characterized by a high, near-continuous rampart. If this is so, what was the fate of the "missing" spatter falling to the south? We propose that two mechanisms removed spatter clasts down slope from the fissure. Proximally, pyroclasts falling within 20 m of the fissure to the south formed spatter-fed flows and within 10 m to the north became impounded lava; in both cases any sense of pyroclastic "identity" was lost. Further downslope (>20 m) on the southern side, spatter fell as discrete clasts but was rafted away on these moving flows. The local southern preservation of pyroclasts on tree molds and paleohighs is proof that distal material fell cooler in this region and could be locally preserved. A total absence of spatter on the lava flow today clearly indicates that flows continued moving after the cessation of fountaining. Upslope, to the north of the fissure (>10 m), a volumetrically minor amount of spatter fed lava was both impounded by the fountains and occasionally flowed around the ramparts (which were able to form and grow because the lava could not readily flow to the south).

Figure 9 shows schematic snapshots through the eruption and the physical processes that we believe led to the near-absence of ramparts on the south side of the fissure. Phase 1 low fountains (Swanson et al. 1979) fed early lava that drained downslope southward, carrying away most of the early spatter as it was deposited (Fig. 9a–b). Some spatter congealed on branches of trees, and lava engulfed tree bases,

Fig. 9 Westward cartoon series showing progression and formation of asymmetrical spatter ramparts. For simplicity, details of subsurface structures (i.e., tree roots, previous lava flows, etc.) are not shown. **a–d** Pyroclasts are color coded (*orange* hot, *red* mod, *gray* cool) and *arrows* in the lava show flow direction. For **a–d** *black lines* around tree trunks are tree mold crusts both within the spatter rampart to the north (right) and in the lava flow field (left and center). **a** Fissure initiation in phase 1. **b** Lava rapidly engulfs the forest as magma flux and fountain height increases during phase 1. Tree mold and rampart formation begins, trees near fissure start to burn, and lava flows transport spatter downslope. **c** During phase 2, peak flux creates dynamically ponded lava flows. Ramparts and tree molds continue to grow, trees continue to be incinerated, and lava drainage pathways stabilize. A lava bench (*thick black line*) forms around the top of tree molds and on pathway margins (not depicted). Spatter is rafted downslope, unless it lands on a tree mold, where it accumulates (*gray*). **d** Incremental fountain decline in Phase 3 allowed the lava flow level to drop in a stepwise fashion, creating secondary/tertiary shelves (not depicted). Any remaining spatter on the lava was transported downslope. North of the lava divide, lava drains back into the fissure after fountain cessation. **e** *Dashed line* indicates where a southern rampart would have been located if fully constructed. Present topography on the surface of the lava flow is shown by the *heavy black line*
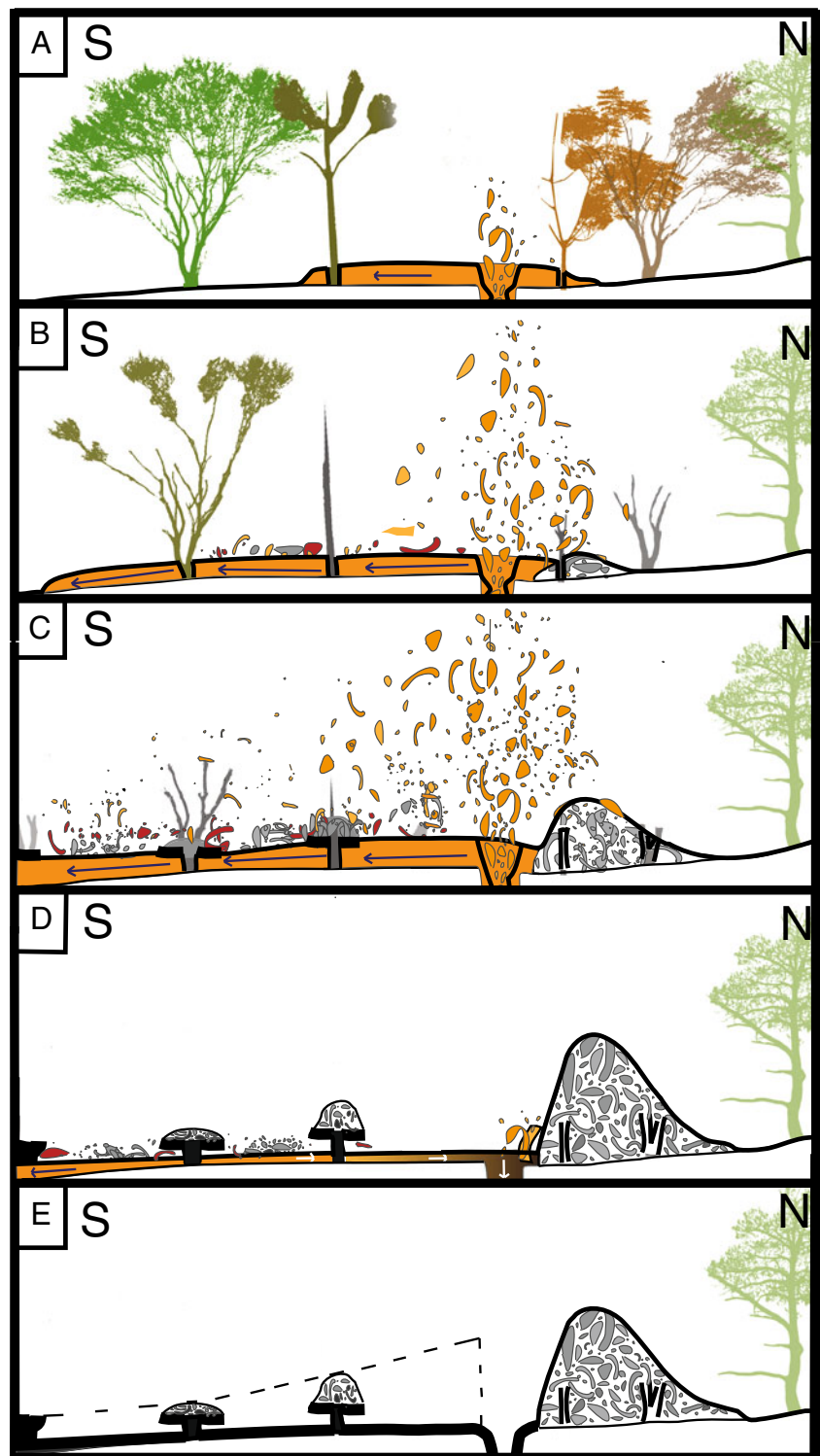
with heat from the newly formed lava crust igniting some trees. Increasing mass eruption rate during phase 1 caused dynamic ponding of the lava flow, burying the remaining trees more deeply, allowing stable crusts to form and attach to the tree molds. Spatter fell continuously beyond 20 m from the fissure but was transported downslope on the flowing lava, except where it landed on the stable crusts anchored to tree molds or other topographical high points (Fig. 9c). With waning discharge rate, the level of the lava flow dropped (Fig. 9d), exposing the spatter-covered mounds at heights of 1–2 m above the present ground surface (Fig. 9e).

The asymmetry of other rampart deposits is covered only fleetingly in the literature. For Kīlauea fissure eruptions, typically the cumulative vent length (e.g., fissure length) is

stated along with a phrase to the effect that "a rampart was constructed." There is generally no discussion of whether the rampart(s) is/are a paired unit or a single asymmetrical feature as seen at Mauna Ulu. However, asymmetrical ramparts on Kīlauea are not confined to the 1969 eruption (e.g., October 1963, Moore and Koyanagi 1969; December 1965, Fiske and Koyanagi 1968), but other fissures have not produced asymmetrical deposits to the same extreme that is observed at Mauna Ulu. In addition, accounts of fissure eruptions in Japan, Italy, and Iceland also simply acknowledge that ramparts formed, but give no dimensions or detailed analysis. In this paper, we have presented new data sets to better quantify, understand, and model the dynamics and products of low Hawaiian fissure fountains.

Conclusions

The fissure eruption of May 24, 1969 illuminates a misconception that explosive eruptions always produce thicker deposits downwind from vent. Preserved deposit thicknesses during low fountaining eruptions reflect many influences, including ground slope, the presence or absence of coeval lava flows, accumulation versus deposition rates, local topographic relief, and the wind field. On Kīlauea, symmetrical (paired) ramparts are not always formed during fissure eruptions. For fountaining eruptions of fluid magmas, like basalt, a dynamic balance always exists between processes promoting rampart/cone growth and processes favoring removal of tephra via coeval lava flows. The ramparts of May 24, 1969 show that this eruption balanced at the cusp between explosive (pyroclastic) and effusive activity.

References

Aramaki S, Utsu T, Watanabe H, Ida Y, Yukutake T, Notsu K, Shimozuru D (1988) In: S Aramaki (ed). The 1986–1987 eruption of Izu-Oshima volcano. Earthquake Research Institute: University of Tokyo; pp 1–61

Behncke B, Neri M (2003) The July–August 2001 eruption of Mt. Etna (Sicily). Bull Volcanol 65(7):461–476

Bonaccorso A, Bonforte A, Calvari S, Del Negro C, Di Grazia G, Ganci G, Neri M, Vicari A, Boschi E (2011) The initial phases of the 2008–2009 Mt. Etna eruption: a multi-disciplinary approach for hazard assessment. J Geophys Res 116:B03203. doi:10.1029/2010JB007906

Fiske RS, Koyanagi RY (1968) December 1965 eruption of Kilauea volcano, Hawaii. U S Geol Surv Prof Pap 607

Heliker C, Swanson DA, Takahashi TJ (2003) The Puʻu ʻŌʻō – Kūpaianaha Eruption of Kīlauea Volcano, Hawaiʻi: The First 20 Years. U S Geol Surv Prof Pap 1676

Hon K, Kauahikaua J, Denlinger R, Mackay K (1994) Emplacement and inflation of pahoehoe sheet flows: Observations and measurements of active lava flows on Kilauea Volcano, Hawaii. Geol Soc Am Bull 106:351–370. doi:10.1130/0016-7606(1994)106<0351:EAIOPS>2.3.CO;2

La Delfa S, Patane G, Clocchiatti R, Joron JL, Tanguy JC (2001) Activity of Mount Etna preceding the February 199 fissure eruption: inferred mechanism from seismological and geochemical data. J Volcanol Geotherm Res 105(1–2):121–139

Macdonald GA, Abbott AT, Peterson FL (1983) Volcanoes in the sea: the geology of Hawaii, 2nd edn. University of Hawaii Press, Honolulu

Moore JG, Koyanagi RY (1969) The October 1963 eruption of Kilauea volcano, Hawaii. U S Geol Surv Prof Pap 614-c

Moune S, Sigmarsson O, Schiano P, Thordarson T, Keiding JK (2012) Melt inclusion constraints on the magma source of Eyjafjallajokull 2012 flank eruption. J Geophys Res 117(B00C07). doi:10.1029/2011JN008718

Parfitt EA (2004) A discussion of the mechanisms of explosive basaltic eruptions. J Volcanol Geotherm Res 134(1–2):77–107. doi:10.1016/j.jvolgeores.2004.01.002

Parfitt EA, Wilson L (1995) Explosive volcanic eruptions IX: the transition between Hawaiian-style lava fountaining and Strombolian explosive activity. Geophys J Int 121:226–232

Parfitt EA, Wilson L, Neal CA (1995) Factors influencing the height of Hawaiian Lava fountains: implications for the use of fountain height as an indicator of magma gas content. Bull Volcanol 57(6):440–450. doi:10.1007/BF00300988

Peterson DW (1969) Kilauea volcano eruption. Bull Volcan Erupt Volcanol Soc Jap 10:11

Pyle DM (1989) The thickness, volume, and grainsize of tephra fall deposits. Bull Volcanol 51(1):1–15

Richter DH, Eaton JP, Murata KJ, Ault WU, Krivoy HL (1970) Chronological narrative of the 1959–1960 eruption of Kilauea Volcano, Hawaii. U S Geol Surv Prof Pap 537-E:El-E73

Slezin YB (2003) The mechanism of volcanic eruptions (a steady state approach). J Volcanol Geotherm Res 122:7–50

Stevens NF, Murray JB, Wadge G (1997) The volume and shape of the 1991–1993 lava flow field at Mount Etna, Sicily. Bull Volcanol 58(6):449–454

Stovall WK, Houghton BF, Harris AJL, Swanson DA (2008) A frozen record of density-driven crustal overturn in lava lakes: the example of Kilauea Iki, 1959. Bull Volcanol 71(3):313–318. doi:10.1007/s00445-008-0225-y

Sumner JM (1998) Formation of clastogenic lava flows during fissure eruption and scoria cone collapse: the 1986 eruption of Izu-Oshima volcano, eastern Japan. Bull Volcanol 60(3):195–212

Swanson DA, Jackson DB, Duffield DA, Peterson DW (1971) Mauna Ulu eruption, Kilauea volcano. Geotimes 16(5):12–16

Swanson DA, Duffield DA, Jackson DB, Peterson DW (1979) Chronological narrative of the 1969–71 Maun a Ulu eruption of Kilauea volcano, Hawaii. U S Geol Surv Prof Pap 1056

Tilling RI, Christiansen RL, Duffield WA, Endo ET, Holcomb RT, Koyanagi RY, Peterson DW, Unger JD (1987) The 1972–1974 Mauna Ulu eruption, Kilauea Volcano: an example of quasi-steady-state magma transfer. U S Geol Surv Prof Pap 1350:405–469

Vergniolle S, Jaupart C (1990) Dynamics of degassing at Kilauea Volcano, Hawaii. J Geophys Res 95(B3):2793–2809

Vergniolle S, Mangan M (2000) Hawaiian and Strombolian eruptions. In: Sigurdsson H (ed) Encyclopedia of volcanoes. Academic, San Diego, pp 447–461

Walker GPL (1973) Explosive volcanic eruptions—a new classification scheme. Int J Earth Sci 62(2):431–446. doi:10.1007/BF01840108

Wilson L (1980) Relationships between pressure, volatile contents, and ejecta velocity in three types of volcanic explosions. J Volcanol Geotherm Res 8(2–4):297–313

Wilson L, Head J (1981) Ascent and eruption of basaltic magma on the Earth and Moon. J Geophys Res 86(B4):2871–3001

Wilson CJN, Houghton BF (2000) Pyroclastic transport and deposition. In: Sigurdsson H (ed) Encyclopedia of volcanoes. Academic, San Diego, pp 545–554

Wolfe EW, Neal CA, Bamks NG, Duggan TJ (1988) The Puu Oo eruption of Kilauea volcano, Hawaii: episodes 1 through 20, January 3, 1981 through June 8, 1984. U S Geol Surv Prof Pap 1463